



Water Resources Research

RESEARCH ARTICLE

10.1002/2017WR020543

Kev Points:

- A thermal tracer tomography experiment is presented, using pulse injection signals
- The obtained temperature breakthrough curves are interpreted with travel time-based tomographic inversion
- The reconstructed tomogram is compared to geophysical and hydraulic experiments for validation

Supporting Information:

• Supporting Information S1

Correspondence to:

M. Somogyvári, mark.somogyvari@erdw.ethz.ch

Citation:

Somogyvári, M., and P. Bayer (2017), Field validation of thermal tracer tomography for reconstruction of aquifer heterogeneity, *Water Resour. Res.*, *53*, 5070–5084, doi:10.1002/2017WR020543.

Received 6 FEB 2017 Accepted 31 MAY 2017 Accepted article online 7 JUN 2017 Published online 26 JUN 2017

Field validation of thermal tracer tomography for reconstruction of aquifer heterogeneity

Márk Somogyvári¹ and Peter Bayer¹,2 🕞

¹Department of Earth Sciences, ETH Zurich, Zurich, Switzerland, ²Institute for New Energy Systems, Technische Hochschule Ingolstadt, Ingolstadt, Germany

Abstract In the summer of 2015, a series of thermal tracer tests were conducted at the Widen field site in northeast Switzerland to validate travel time-based thermal tracer tomography for reconstruction of aquifer heterogeneity. Repeated thermal tracer tests and distributed temperature observations were used to obtain a multisource/multireceiver tomographic experimental setup. After creating forced hydraulic gradient conditions, heated water was injected as a pulse temperature signal via a double-packer system. With this solution, long temperature recovery periods were not required between the repeated injections at the expense of smaller observed temperatures. The recorded temperature breakthrough curves delivered a tomographic travel time data set that was inverted assuming advection-dominated condition. The obtained hydraulic conductivity tomogram for a small aquifer profile is validated with the results of the findings from previous field investigations at the same site. The reconstructed profile confirms the presence of a thin sand layer with low permeability and reveals a previously unknown low-permeable zone close to the bottom of the aquifer. The inverted hydraulic conductivity values also correspond with those from previous tracer tests. Thus, the results of this study demonstrate the potential of thermal tracer tomography for resolving structures and transport characteristics of heterogeneous aquifers.

1. Introduction

Conventional single tracer tests in groundwater are integrative field investigation methods. They allow estimating average flow and transport properties of an aquifer volume [Yeh and Zhu, 2007]. In contrast, geophysical imaging can capture subsurface heterogeneity by providing the distribution of electric conductivities, radar, or seismic velocities. However, it is difficult to relate such geophysical parameters to hydraulic properties without additional hydraulic measurements [Linde et al., 2006]. The rationale of tracer tomography is to combine tracer techniques with imaging methods. Tracers are injected in order to derive direct estimates of flow and transport parameters. Spatial heterogeneity of these parameters is resolved by applying multiple tracers in a tomographic setup similar to geophysical measurements. Here multiple different tracer injection points (sources) and multiple observation points (receivers) are used to capture the tracer breakthroughs at different locations and to delineate preferential pathways. Sources and receivers can be represented by different injection and observation wells, or, for vertical reconstruction of aquifer heterogeneity, they are situated at different levels in wells.

Hydraulic tomography is based on a similar principle by using the propagation of pressure signals generated by short-term pumping or slug tests [Butler et al., 1999]. As these tests can be performed with similar instrumentation as for classic hydraulic testing, hydraulic tomography is well explored today [Vasco et al., 2000; Brauchler et al., 2003, 2013b; Cardiff et al., 2009; Illman et al., 2009; Berg and Illman, 2011; Hu et al., 2015]. Using tracers instead of hydraulic signals offers new opportunities, because tracer tests can identify directly preferential transport pathways, and they can be combined with hydraulic tomography in joint inversion procedures. Furthermore, the use of different types of tracers with different transport properties can reveal additional characteristics of the subsurface such as heterogeneity of matrix exchange surface or localization of nonaqueous phase liquids [Feehley et al., 2000; Yeh and Zhu, 2007; Zhu et al., 2009; Illman et al., 2010; Wagner et al., 2014].

Inversion algorithms from seismic tomography can be directly used to interpret tracer tomography data sets [Vasco and Datta-Gupta, 1999]. Tracer tomography is capable of characterizing porous [Jiménez et al.,

 $\ensuremath{\mathbb{G}}$ 2017. American Geophysical Union. All Rights Reserved.

2016] and fractured media [Vasco and Finsterle, 2004; Brauchler et al., 2013a]. Datta-Gupta et al. [2002], Yeh and Zhu [2007], Zhu et al. [2009], and Illman et al. [2010] have demonstrated its suitability for identifying different liquid phases (such as dense nonaqueous phase liquids) in an aquifer. Field applications with multiple tracers are scarce, yet one has been presented by Jiménez et al. [2016] using different dye tracers and a pilot-point-based inversion procedure to reconstruct an aquifer profile. This lack of field tests may be due to the demanding experimental design and instrumentation, the need for in situ tracer monitoring or repeated multilevel sampling, and the time and cost for carrying out a full experiment. Therefore, tracers are more commonly applied to validate or complement other hydrogeological or hydrogeophysical field tests [Sharmeen et al., 2012; Dorn et al., 2013; Jiménez et al., 2015; Sanchez-León et al., 2016].

In recent years, heat as an actively injected tracer has raised increasing attention [Anderson, 2005; Saar, 2011; Rau et al., 2014]. Irvine et al. [2013] pointed out that using heat over solute tracers provides better approximation of groundwater velocity at the expense of detecting heterogeneities. In comparison to the transport of solute tracers, conductive heat transport into the aquifer matrix can play a substantial role. This slows down the tracer transport [Shook, 2001] and the tracer signals are more attenuated since a large part of the injected energy is used to heat up the aquifer matrix. Due to the high diffusivity in comparison to solute tracers and the potential influence of background temperature perturbations, heat is not considered an ideal tracer [Xue et al., 1990; Irvine et al., 2013; Xie et al., 2015]. Aside from this, physical parameters such as hydraulic conductivity, K, are dependent on temperature. Water density and viscosity changes as temperature increases, and density driven flow is induced. Still, heat has some appealing features that make it favorable in many tracer applications, especially for tomography.

First, available temperature monitoring techniques can measure the evolution of temperature in situ and real time, at high accuracy and at low cost. Multilevel observations are obtained by using multiple temperature sensors with fixed locations in the borehole or by using a distributed temperature measurements system (DTS). DTSs use fiber optic cables for observations providing high spatial resolution [Bense et al., 2016]. Temperature sensors are easier to use, cheaper and the better choices when point measurements are sufficient [Benz et al., 2015; Doro et al., 2015]. Second, natural background temperature variations are often small, much smaller than changes induced by tracer tests. If necessary, background temperature trends can be filtered out using preliminary baseline measurements or frequency filtering. It is even possible to exploit the natural temperature differences inside the aquifer for investigations. This approach is especially suitable in fractured media where abrupt temperature changes can be caused by modifying the existing flow conditions. This technique has been used for fracture detection and characterization by Klepikova et al. [2014]. Third, despite the strong influence of heat diffusion and density effects, thermal tracer testing in heterogeneous formations allows for the delineation of preferential pathways, where heat transport is dominated by advection [Irvine et al., 2013; Wagner et al., 2014; Djibrilla Saley et al., 2016]. In our earlier theoretical study [Somogyvári et al., 2016], we have shown that by using a travel time-based inversion technique, the influence of density changes, viscosity variations, and diffusion effects is minimized and a wide application window for thermal tracer tomography is available.

Thermal tracer techniques can be categorized by the heat tracer source used. In the literature, four main source signal types are found, which create different response signals at an observation point (Figure 1). The most common source type is the step injection. Here the temperature at the injection point follows a Heaviside-signal shape (Figure 1a). This continuous thermal tracer injection can be realized by using a natural source with small temperature difference, for example water from another aquifer or an adjacent surface water body. Here periodically changing temperature may be used for injection. In this case, the phase shift between the injected and observed signal can be investigated (Figure 1c) [Keys and Brown, 1978]. A more common approach is to use an on-site heating device to produce warm water continuously [Molz et al., 1981; Palmer et al., 1992; Vandenbohede et al., 2011; Irvine et al., 2013; Wildemeersch et al., 2014; Colombani et al., 2015; Doro et al., 2015; Cherubini et al., 2017], because temperature changes can be self-defined and higher (Figure 1a). Although observations from step injection signals are easier to detect, their technical implementation with active heating devices is difficult. Maintaining a constant temperature injection signal for a long period requires a large amount of energy and reliable operation of the heating system. An alternative is heating up a small volume of water, which is then injected as a Dirac pulse signal [Wagner et al., 2014; Djibrilla Saley et al., 2016] (Figure 1b). Pulse signals are standard in solute or particle tracer tests where a limited amount of tracer solution is available or needed. For thermal tracer tests, it is important that the

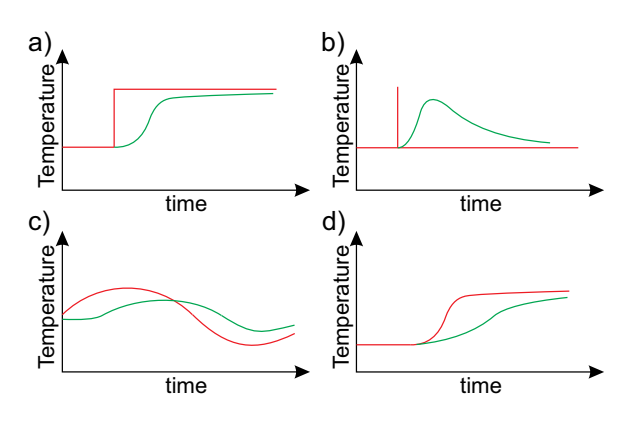


Figure 1. Different injected thermal tracer signals and observed responses. Red curves: injection signals, green curves: observed response signals. (a) Heaviside signal with continuous thermal tracer injection, (b) pulse injection, (c) injection of natural water with periodic temperature changes, and (d) in situ conductive heat source.

injection volume and the temperature difference of the introduced water are sufficient to achieve detectable temperature changes in the observation well. Another option of generating temperature anomalies is in situ heating with a submersible heat source (e.g., heating cable) [Bakker et al., 2015; Coleman et al., 2015; Seibertz et al., 2016]. Here electrical energy is directly converted to heat in situ with a conductive source (Figure 1d). No fluid injection is required for this variant if there is natural groundwater flow. However, the amount of energy introduced by heating is limited and the generated temperature signal will be relatively smooth, making it difficult for instance, to calculate tracer travel times.

Field applications of heat signals in tomo-

graphic arrangement are scarce. *Doro et al.* [2015] focused on the design issues of thermal tracer tomography and reported a tomographic measurement campaign. However, no detailed aquifer characterization has been done using the collected data. Among the procedures available for tomographic inversion, geostatistical and travel time methods have been suggested. The procedure by *Schwede et al.* [2014] assumes that the spatial distribution of log-K follows a random space function with known correlation. Also, the definition of midrange clusters is recommended because the inversion is computationally intensive. Alternatively, computationally efficient travel time-based inversion has been suggested by *Somogyvári et al.* [2016]. Travel time-based tomographic inversion methods exploit the similarities between the propagation of tracer fronts and seismic pressure waves [*Vasco and Datta-Gupta*, 1999; *Brauchler et al.*, 2013a]. Available solvers yield the distribution of the mean tracer velocities, which can then be converted to a *K* distribution. The potential and limitations of thermal tracer tomography were shown by means of two-dimensional (2-D) and three-dimensional (3-D) synthetic examples [*Somogyvári et al.*, 2016].

The objective of this study is to further develop the travel time-based thermal tracer tomography concept presented in *Somogyvári et al.* [2016] and to validate it under field conditions. In the following, the theoretical background is provided first. Also, we present findings from preliminary field testing, which were used to prepare the setup of the full experiment. Based on this, a new thermal tracer tomography design is presented using pulse injections to minimize the temperature recovery times in the aquifer between sequential injections. The inversion methodology, originally developed for continuous thermal tracer injections, is adjusted to the use of pulse signals. We conclude with the results from field application and inverted *K*-profiles, which are compared to findings from earlier investigations at the site.

2. Methodology

2.1. Travel Time-Based Tomography

While heat diffusion obscures the contribution of advective transport in case of small flow velocities, it may be neglected in regimes with fast groundwater flow. Assuming that heat transport is dominated by advection, the properties of thermal transport can be related to the hydraulic properties of the aquifer. In this case, the travel times of thermal tracers can be directly linked to hydraulic conductivity, *K* [Somogyvári et al., 2016]. The propagation of a thermal tracer front between two points can be described by modifying the original line integral formulation of *Vasco and Datta-Gupta* [1999] for tracer tomography by introducing the thermal retardation factor (*R*).

$$t_{tt}(x_r) = \int_{x_r}^{x_r} \frac{ds}{v_{tt}(s)} = \int_{x_r}^{x_r} \frac{\phi(s)}{K(s)i(s)} ds$$
 (1)

Here $t_{tt}(x_r)$ is the travel time of the thermal tracer at the receiver (x_r) , x_s is the location of the heat source, ϕ is aquifer porosity, and i is the local hydraulic gradient. Equation (1) is known as the travel time equation (or

eikonal equation) of the thermal front between the source and receiver. The thermal retardation factor, R, describes the lag in the travel time of heat relative to a nonretarded solute. It depends on the aquifer porosity as well as on the heat capacities of the water and the aquifer matrix $(R=C_m/(\phi C_w))$. While the values of K of porous aquifers typically span orders of magnitude, variability in porosity, thermal retardation, and hydraulic gradient are commonly much smaller. Thus, the tracer travel time is most sensitive to an unknown distribution of K, and the other variables of equation (1), ϕ , R, and i are approximated by constant values. As these parameters span a small range of values, these approximations only introduce small errors into the results [Somogyvári et al., 2016].

The line integral of equation (1) describes the relationship of the travel time to the velocity distribution along one transport trajectory. In a tomographic setup, multiple transport pathways dissect the aquifer. The velocity distribution of the investigated volume determines the tracer travel times. The set of travel time line integrals form the inverse problem. Inverting all the travel time equations together, this velocity distribution can be calculated. As the same formulation is used to describe the propagation of seismic signals or electromagnetic waves in geophysical tomography, standard inversion methods are available to estimate the velocity field. In this study, the SIRT algorithm is deployed to invert the travel times of the heat tracer, implemented in the software GeoTOM3D [Jackson and Tweeton, 1996]. The SIRT algorithm calculates the transport trajectories over a velocity grid and iteratively updates the values of the grid cells until the simulated and observed travel times match. As a result, the mean tracer velocity distribution (velocity tomogram) is obtained, which can then be converted to a K-field (K-tomogram) according to equation (1). Instead of solving the problem over a regular grid, the staggered grid method is applied in this study [Vesnaver and Böhm, 2000] in line with related travel time-based hydraulic tomography applications [Jiménez et al., 2013; Hu et al., 2015; Somogyvári et al., 2016]. The inverse problem is solved over multiple coarse grids, shifted horizontally and vertically. This reduces the bias of the inversion caused by the relation of the source-receiver locations to the grid geometry. The final tomogram is computed as the average of all grids, with a final resolution equal to the used displacements. The main advantage of this method is that it provides higher-resolution tomogram without compromising the stability of the inversion.

As the inversion only uses information from the transport pathways, the quality of the tomogram is variable in space. The reliability of the different parts of the tomogram is assessed by calculating the null-space energy map [Brauchler et al., 2013a, 2013b; Jiménez et al., 2013; Somogyvári et al., 2016]. The null-space energy map is computed by singular value decomposition (SVD) of the tomographic matrix, which contains the length of each inverted transport trajectory in each grid cell. The null-space energy map values range between 0 and 1, whereas higher null-space means less reliable pixels. The null-space energy map is used to mask out nonreliable pixels from the result, especially zones which are not reached by the inverted tracer trajectories.

2.2. Breakthrough Time Calculation

The travel time-based thermal tracer tomography inversion presented in *Somogyvári et al.* [2016] uses continuous thermal tracer injections for source signals. It was shown that it is advantageous to use earlier diagnostic times of breakthroughs to reduce experimental times and distortions caused by thermal diffusion. The breakthrough times were assigned to the time when the first temporal derivative of the temperature peaked at the observation point. By this, the tomographic approach revealed to be especially suitable to reconstruct highly conductive zones in an aquifer, and applicable in a broad range of geological and technical conditions. This was synthetized in the form of an application window in our numerical study [*Somogyvári et al.*, 2016].

For this study, pulse injection signals were chosen due to practical reasons and after preliminary field testing. This requires a different approach for breakthrough time calculation. When pulse injection is used, the travel time of the thermal tracer is the time when the temperature at the observation point peaks. Since heat is a relatively slow tracer [Shook, 2001], this time can be late—requiring long observation times, which may be prohibitive for tomographic setups with multiple sequential applications. The derivative of temperature peaks much earlier, and relating the derivative peak to the travel time could help to reduce the required experimental times. The corresponding procedure is developed in the following.

The thermal response of a thermal pulse (instantaneous heat injection) in an advective-diffusive and one-dimensional (1-D) environment can be analytically formulated as

1944/7973, 2017, 6, Downloaded from https://agupubs.onlinelibrary.wiley.com/doi/10.1002/2017WR020543 by Cochrane Germany, Wiley Online Library on [22/08/2023]. See the Terms and Conditions (https://onlinelibrary.wiley

$$T(x,t) = \frac{Q_{in}^*}{4\pi Dt} \exp\left(-\frac{(x-ut)^2}{4Dt}\right)$$
 (2)

This equation is modified following the available solution for solute tracers [Evans, 1983]. This 1-D approximation is valid in the close vicinity of the observation point. $Q_{in}^* = \frac{Q_{in}}{V_uC}$ represents the heat source term, that is, the amount of heat injected over a unit volume V_u given the local heat capacity C. D is the thermal diffusivity. The first temporal derivative reads as

$$\frac{dT(x,t)}{dt} = -\frac{Q_{in} * \exp\left(-\frac{(x-ut)^2}{4Dt}\right) (u^2 t^2 + 4Dt - x^2)}{16\pi Dt^2}$$
(3)

The thermal breakthrough time is defined as the time when the temperature peaks:

$$\frac{dT(x,t)}{dt} = 0 (4)$$

while the "breakthrough time" of the derivative curve is

$$\frac{d^2T(x,t)}{dt^2} = 0 ag{5}$$

The second derivative of the temperature (equation (2)) reads as

$$\frac{d^2T(x,t)}{dt^2} = \frac{Q_{in}^* \exp\left(-\frac{(x-ut)^2}{4Dt}\right) (32D^2t^2 + 8Du^2t^3 - 16Dtx^2 + u^4t^4 - 2u^2t^2x^2 + x^4)}{64\pi D^3t^5}$$
(6)

The analytical solutions of equations (4) and (5) are complex, making it difficult to use in any further deduction. However, by neglecting the terms with higher order velocities (because groundwater flow is slow), the solutions can be simplified to

$$t(T'=0) = \frac{x}{4D} \tag{7}$$

$$t(T''=0) = \frac{2x^2 - \sqrt{2}x^2}{8D} \tag{8}$$

Relating the breakthrough time to the peak time of the derivative with a transformation factor (α) is a technique used earlier for step signals in *Somogyvári et al.* [2016] and *Brauchler et al.* [2003]. The transformation gives the relation between the breakthrough time, t_{BT} and the derivative time, t_{DT} :

$$t_{BT} = \alpha t_{DT} \tag{9}$$

Hence, the travel time of the thermal tracer can be expressed as a fraction of the time of the derivative peak, with a transformation factor computed as

$$\alpha = \frac{t(T''=0)}{t(T'=0)} = 1 - \frac{1}{\sqrt{2}}$$
 (10)

Note that this expression is only valid with the strong assumption that the seepage velocity is small. Aside from this, t=0 should be the time when the temperature starts to increase at the observation point similar to the early time diagnostics method in *Somogyvári et al.* [2016]. The transformation procedure is illustrated in Figure 2a.

To validate this methodology, temperature breakthrough curves (BTCs) recorded in the subsequent field experiment are analyzed ex ante. The observed breakthrough times are compared with the simulated ones from the derivative peak (according to equations (9) and (10)), as shown in Figure 2b. The derivative-based breakthrough times are always larger than the observed breakthrough times, which is problematic especially at smaller travel times. This limits the reliability of the inversion method. To overcome this, the derivative-based breakthrough times are only used to complement the data set, when a thermal tracer test is terminated before the full BTC is captured. However, when the complete one was recorded, the measured peak breakthrough time was chosen. It is also possible that in the worst case, no temperature response is

conditions) on Wiley Online Library for rules of use; OA articles are governed by the applicable Creative Commons License

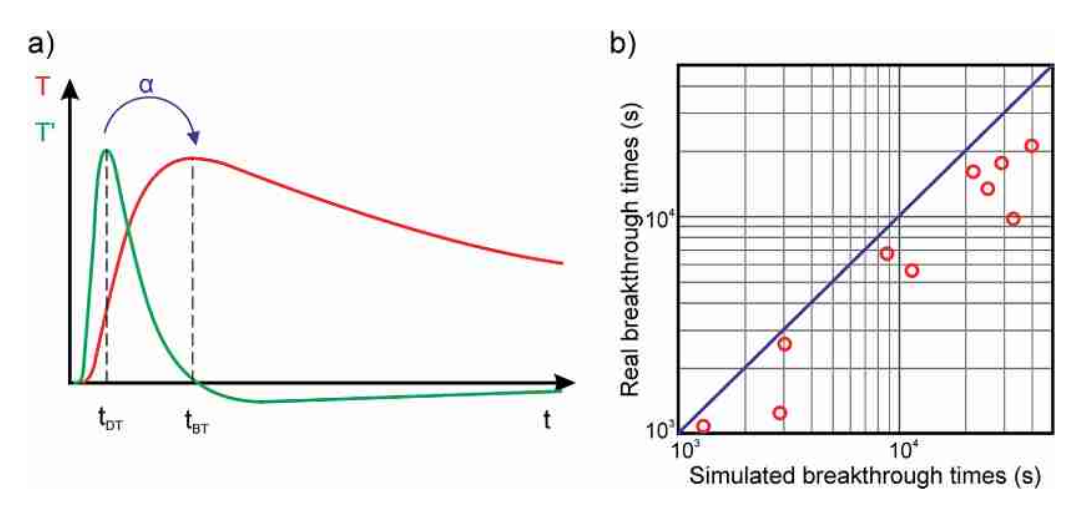


Figure 2. Breakthrough time calculation from temperature derivatives. (a) Methodology of calculation. α is the transformation factor, t_{DT} is the peak time of the derivative temperature (T), and t_{BT} is the breakthrough time of the temperature (T). (b) Comparison of the real breakthrough times versus the simulated ones using full recorded temperature breakthrough curves.

recorded at all, and thus no breakthrough time can be determined. However, this observation is also worthwhile, indicating limited connectivity between source and receiver or low-K zones in the aquifer. As travel time inversion formally only use breakthrough times as input parameters, such source-receiver combinations are included here by assigning virtual travel times. These virtual travel times are calculated assuming a straight transport trajectory between source and receiver and taking the lowest value of K estimated based on equation (1). The lowest K value is calculated from the largest registered travel time of the thermal tracer. With this extension of the data set, a better reconstruction of the aquifer is expected, but with the added risk of wrong low-K values in the tomogram.

3. Field Site and Test Design

3.1. Widen Field Site

The Widen field site is situated in the valley of the Thur River, in northeast Switzerland close to the city of Zurich (Figure 3). The field site was initiated in the summer of 2008. It has been investigated in several field campaigns [Doetsch et al., 2010; Coscia et al., 2011; Jiménez et al., 2016; Deuber et al., 2017] and used for education at ETH Zurich.

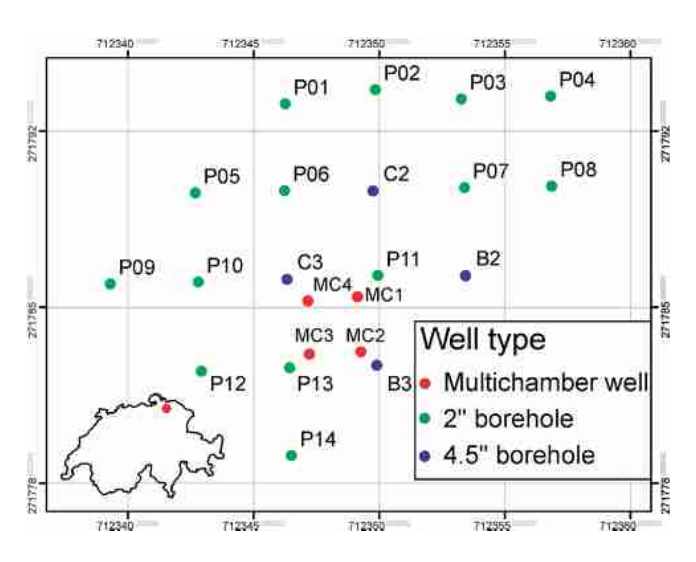


Figure 3. Well configuration at the Widen field site; the location in Switzerland is highlighted in the map at the lower left.

The site hosts a shallow aquifer dominated by the Thurtalschotter formation, a 7 m thick fluvial gravel layer (Figure 4). Below the aguifer bottom at around 10 m depth, low-permeable lacustrine sediments are found, while the aquifer is covered with around 3 m thick alluvial sand sediments. The depth of the aquifer bottom is variable within the field site as a consequence of fluvial erosion during deposition (e.g., between wells P11 and MC1). The aguifer is connected to the River Thur, and strong precipitation events cause changes in the water table. Normally, the water table is in the gravel formation yielding unconfined conditions. During flood events, the aquifer becomes semiconfined as the groundwater reaches the overlying sand. The

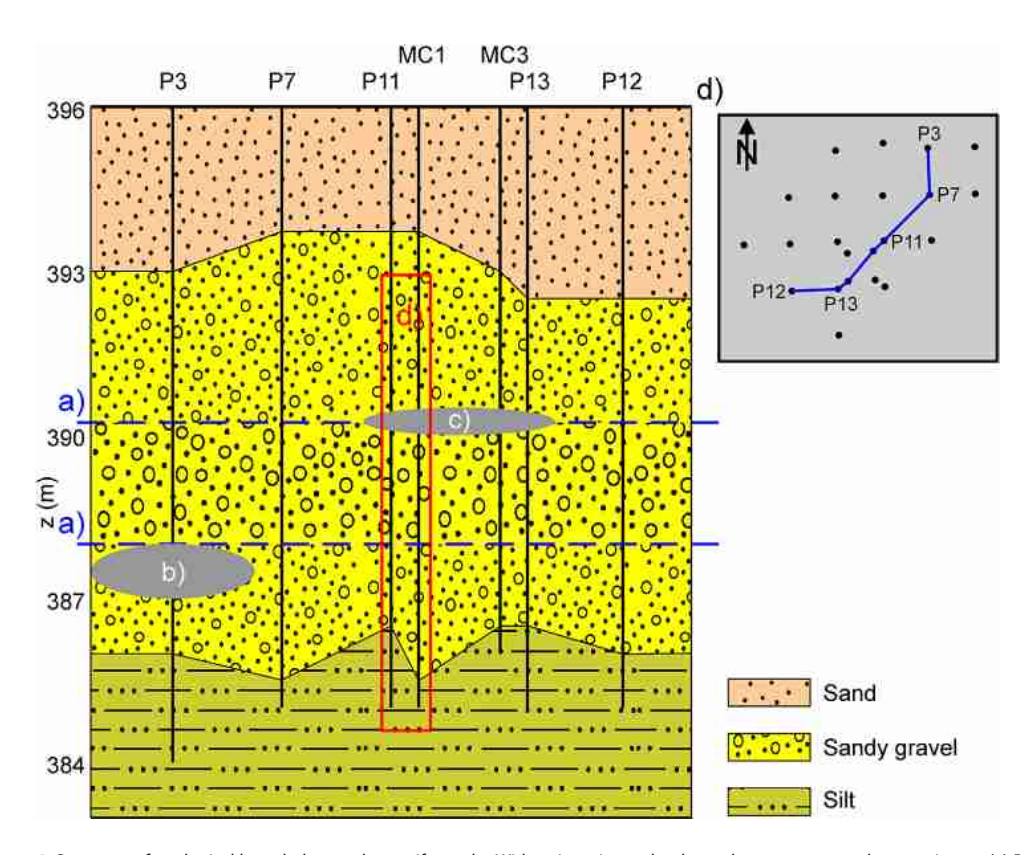


Figure 4. Summary of geological knowledge on the aquifer at the Widen site prior to the thermal tracer tomography experiment. (a) Resistivity discontinuities in the aquifer bordering a high permeability layer, suggested by hydraulic tests and ERT measurements [Doetsch et al., 2010; Coscia et al., 2011]. (b) Sand lens known from core logs and slug tests [Jimenez et al., 2016]. (c) Sand layer (or lens) located by solute tracer tomography experiment [Jiménez et al., 2016]. (d) Trace map of reconstructed profile.

general groundwater flow direction is NE-SW, but deviations of up to 45° were experienced in different experiments revealing dynamic hydraulic conditions in the aquifer.

In the heterogeneous Thurtalschotter, sand lenses were found in core logs and by slug tests (Figure 4). *Jiménez et al.* [2016] identified the presence of a thin but extensive sand lens at 390 m level. The exact extent of this sand lens is unknown, but its presence was measured in wells P11 and P13 by slug tests. Geophysical investigations (cross-well ERT) showed that the central zone of the aquifer body between 388 and 390 m has higher electric resistivity than the formation above and below This suggests that the central zone of the Thurtalschotter formation has higher gravel content associated with higher-K. Multilevel slug tests showed a wider zone of high-K between 387 and 390 m, and another high-K zone above the 390 m low-K layer [*Jimenez et al.*, 2016].

The Widen site hosts 22 investigation wells in total (Figure 3). Eighteen boreholes are aligned roughly as points of a rectangular grid (P01–P14, B2, B3, C2, and C3). The boreholes penetrate down to the aquifer base and they are screened through the whole aquifer body. Four of the wells (MC1–MC4) are equipped with multichamber casings (Continuous Multichannel Tubing (CMT)) [Einarson and Cherry, 2002], which facilitate multilevel sampling. Each multichamber well has seven separate tubes inside, screened at seven different depth levels with 10 cm long screens. These wells were used for temperature measurements by installing sensors in each chamber.

3.2. Preliminary Testing

In the summer of 2014, a series of active thermal tracer tests were conducted at the Widen site, to test the continuous injection thermal tracer tomography design under field conditions [Schweingruber et al., 2015]. A high performance diesel fueled water heater was used to produce 60°C water at a flow rate of 0.2 L/s. To minimize temperature variations, the heated water was mixed with cold water in a 120 L volume tank, finally providing a flow rate of 1 L/s at 30°C. We were able to operate this injection system for 60 h, with

variations less than 3°C in the injection temperatures. However, the experiment required constant operation of the heater, which was out of service several times. These short interruptions in the continuous injection caused significant distortions in the recorded BTCs. The heating also required a large amount of fuel to operate, making the experiment expensive. Doro et al. [2015] used a double-packer system to vertically isolate the injection interval of the warm water. Additionally, above and below the injection interval, water at ambient temperature was injected. The additional injections focused the warm water to propagate horizontally in a similar way as laterologs focus the electric currents in borehole geophysics. The setup we used was simpler. The warm water was injected in well P13 (Figure 3) via a double-packer system without any focusing of the heat plume as suggested by Doro et al. [2015]. The injection is switched to cold injection with an estimated rate of 1 L/s after all warm water has been injected. To increase the hydraulic gradient, water extracted from well C2 was reinjected in well P14 with a rate of 3 L/s, generating forced gradient conditions. Temperature differences of over 10°C were observed in the closest observation borehole (MC3) at 1.5 m distance. Other boreholes have showed no or very weak responses, although sensors were capable to detect temperature changes below 0.05°C. This was the effect of the strong natural background flow, which was diverting the heat plume from the observation wells. Measurements after the injection experiment showed that close to the injection well the recovery back to the ambient temperature was very slow. This made it impossible to repeat the thermal tracer test on a subsequent day due to the disturbed initial thermal conditions in the aquifer.

Among the main findings of the preliminary test were that very small temperature changes are measureable in the low-noise subsurface environment. The high experimental costs, the huge risk of technical malfunctions, and the long recovery time motivated us to consider an alternative heat injection procedure. This is explained in the following description of the full-scale tomographic experiment.

3.3. Experimental Setup of Thermal Tracer Tomography

With the experience from the preliminary testing campaign, the tomographic experiment conducted in the summer of 2015 was carefully aligned with the natural groundwater flow direction, and a pulse-type injection signal was employed. Pulse injection is advantageous, because less energy is required for heating than for continuous injection and the aquifer temperature can recover faster. These aspects are especially appealing for tomography, when multiple heat tracer tests are needed, but at the expense of less pronounced signals. Consequently, only a short profile of the aquifer is chosen for the test (P11-MC1, Figure 4). Figure 5 illustrates the experimental configuration. Two Grundfos JP Hydrojet surface pumps were used to maintain the forced gradient flow field in parallel with the ambient groundwater flow. The water extracted from well P12 at a rate of 0.4 L/s was discharged to the river, while the water extracted from P14 was rein-

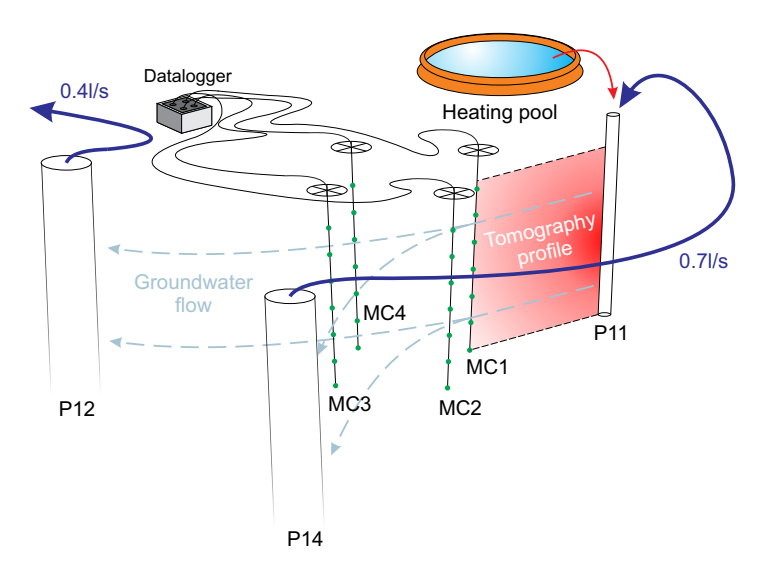


Figure 5. Experimental design of tomographic thermal tracer test: the water for injection is heated up by the sun in an inflatable swimming pool. The ambient groundwater flow is enhanced through a forced gradient setup. The temperature changes are monitored in four multichamber wells, with 1 m vertical resolution.

jected to P11 at 0.7 L/s. Pumping was performed over the full well screen. The reinjection scheme represents a doublet-like setup, which adequately controlled the flow velocity and direction close to the heat injection well (P11). The pumps were started hours before the heat injection in order to reach quasi steady state conditions. By injecting heat via a double-packer system with a screen length of 20 cm, local point injection configuration was approximated.

To minimize the costs of the experiment, water which was taken from well P14 was warmed in three small inflatable swimming pools by direct sunlight [see also Wagner et al., 2014].

Table 1. Details of the Different Thermal Tracer Injections of the Main Experiment				
	Start of	Experiment	Injection	Injection
	Experiment	Duration (h)	Temperature (°C)	Level (m) ^a
Injection 1	13.07.2015 16:06	6	30	389.075
Injection 2	14.07.2015 13:17	7	32	387.3
Injection 3	15.07.2015 13:01	3	32	390.075
Injection 4	15.07.2015 16:06	2	31	391.075
	isolated interval.			

During the sunny summer days of the experiment, 300 L of water were heated up to 30°C in 3–4 h from the ambient 15°C groundwater temperature. Before injection, the water was mixed in a fourth larger swimming pool, and directly injected to P11 over a period of approximately 10 min.

Compared with the duration of hours for the full experiment, this short time interval was approximated as an instantaneous pulse injection. As the injection was performed without any pumping, the injection rate was reduced during warm water injection. This disturbed slightly the flow field for a short period, but it recovered immediately after switching back to cold injection. The tomographic experiment consisted of four individual thermal tracer tests performed in four different injection intervals. The different injection settings of all successive thermal tracer tests during the tomographic experiment are summarized in Table 1. However, the given volumes of water were estimated and were not used for any further analysis.

Although the 15° C temperature difference at injection is over the 8° C limit of buoyancy driven flow given by *Schincariol and Schwartz* [1990], it is expected that the water cools down very quickly close to the injection point due to mixing and diffusion. The tomographic inversion is demonstrated to work at higher temperature differences with much higher injected volumes [*Somogyvári et al.*, 2016]. The latter theoretical study, however, focused on continuous heat injection, and thus the obtained findings cannot be transferred to the heat-pulse application of this work. The estimated thermal Peclét number of the high-K zones of the aquifer is in the range of Pe = 10-100, which denotes that the thermal transport is dominated by advection.

Campbell Scientific 108 temperature sensors with negative temperature coefficients were utilized for temperature measurements. The absolute accuracy of these sensors is smaller than 0.1°C, while temperature changes of 0.01°C were the smallest registered. Note that for travel time-based thermal tracer tomography, the absolute accuracy of sensors is not crucial, as breakthrough times are calculated from relative temperature changes (see Figure 2a). In total, 28 temperature sensors were used, 26 installed in the multichamber wells (7–7 in MC1 and MC3, 6–6 in MC2 and MC4), and 2 additional ones monitored the air and the injection temperature. The temperature measurements were collected and recorded with a Campbell Scientific CR3000 datalogger, with 0.1 Hz sampling rate.

Four thermal tracer tests were conducted over three consecutive days to have minimal changes in the ambient hydraulic conditions. On the first 2 days, one thermal tracer test was executed per day and on the third day, two were performed. The overnight pauses were enough for complete thermal recovery of the aquifer. After the shorter pause of 3 h between the two injections on the last day, increased temperatures were measured, but the thermal breakthroughs could still be measured.

4. Results

4.1. Observations and Data Processing

The temperature observations of the four injection experiments delivered 104 BTCs in total. The BTCs are treated with a low-pass zero-phase filter [Oppenheim and Lim, 1981] to remove high frequency noise from the data. Such short time variations are related to instrument noise. A general feature of thermal tracer tests is that the recorded temperature curves can be well filtered. Natural background temperature trends have much lower frequencies, and disturbances from measurement noise have much higher frequencies than the tracer test signal.

Travel time-based thermal tracer tomography does not use absolute temperature values for the inversion, but rather the travel times are calculated from the relative temperature changes. These time-dependent changes are normalized by the injection temperature, ΔT^* , and shown in Figure 6 for the different injections observed in MC1. In Figures 6b and 6c, the observed temperature responses are not in the same depths as the injections. This is a first indication of inclined preferential flow paths in the Thurtalschotter.

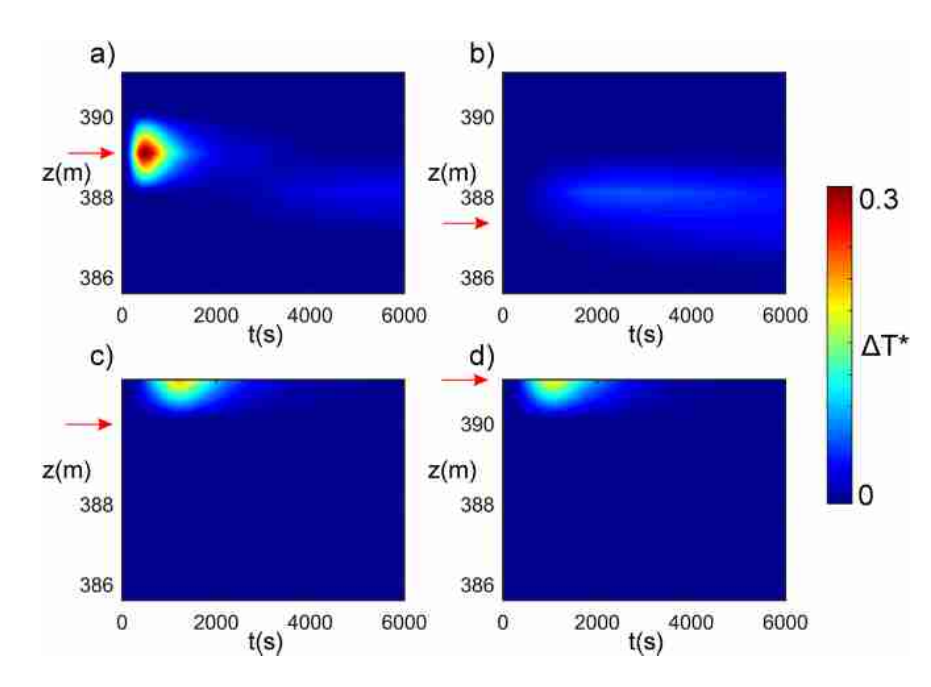


Figure 6. Normalized relative temperature changes (ΔT^*) observed in MC1 borehole after heat tracer injections in four different depths. The temperature differences are normalized by the average injection temperature (20°C). The red arrows mark the depths of injections (sources)

Eleven BTCs were recorded during the tomographic experiment (supporting information Figures S1–S3). Three additional travel times were calculated from temperature derivatives to complement the data set (equation (9)). For the 14 source-receiver combinations without any breakthrough, virtual travel times were estimated from the source-receiver distance. Without these virtual travel times, the reconstruction of low-*K* aquifer zones would be limited. In total, 28 travel times were used as an input for the inversion. The collected BTCs are sufficient to reconstruct the 2-D profile between well P11 and MC1. Further information collected from the other multichamber wells could be used in additional experiments for a more extensive 3D reconstruction.

4.2. Parametrization of Inversion Procedure

An average hydraulic gradient of i=0.005 dipping SW is calculated from head measurements of the four different tests. Further parameter values of the aquifer are taken from the literature and previous investigations at the site. The volumetric heat capacity of water is $C_w = 4.18 \times 10^6 \text{ J/m}^3 \text{ K}$. The rock matrix is considered saturated gravel with a heat capacity of $C_m = 2.2 \times 10^6 \text{ J/m}^3 \text{ K}$ [Stauffer et al., 2013]. An effective porosity value of $\phi = 0.25$ is assigned [Jimenez et al., 2016].

The maximum allowed tracer velocity is constrained in the tomographic solver to keep the inverted tracer velocity values within a realistic range [Somogyvári et al., 2016]. This is especially important for the edges of the inverse model, where due to data sparsity, the method could generate extreme values. The maximum allowed velocity of the inversion is set to 0.0023 m/s. This value is equivalent to $K = 5.5 \times 10^{-2}$ m/s (see equation (1)), given the values for I, R, and ϕ . To calculate virtual travel times, a value of $K = 6 \times 10^{-4}$ m/s is selected based on the largest detected travel times.

The cell size of the solution grids is defined as 1 m \times 1 m. The optimal grid resolution for tomographic inversion has the same number of cells as the number of the inverted travel times [Vesnaver and Böhm, 2000]. Here 30 cells were fit to 28 BTCs. Inversion on higher-resolution grids would lead to instable results due to the ill-posed inverse problem [Aster et al., 2013].

Four times staggering is used, shifted to both vertical and horizontal directions. Accordingly, the problem was solved on 16 different grids in total. The cell size of the final fine resolution grid is 0.25 m \times 0.25 m. The required computational time on an office computer was less than 3 min for the complete tomographic inversion (Intel® CoreTM i7–4770 CPU 4 \times 3.40 GHz).

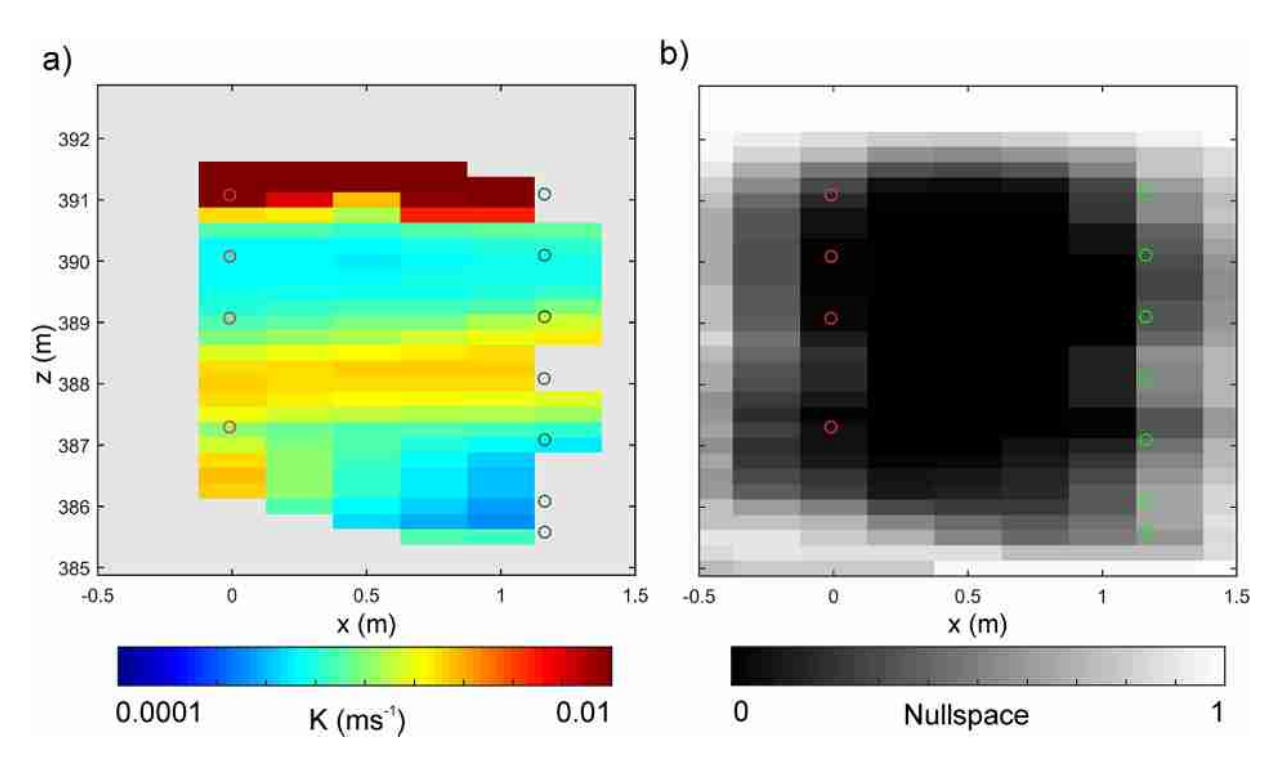


Figure 7. Results of the inversion. (a) Reconstructed hydraulic conductivity tomogram. Red circles are the point injections (sources) at P11 and green circles are the sensor locations (receivers) at MC1. (b) Null-space energy map.

4.3. Inversion Results

The results of the inversion are presented in Figure 7. The reconstructed K values in the tomogram shown in Figure 7a are mostly above 10^{-3} m/s, with no pixel below 10^{-4} m/s. In the tomogram, a low-K layer embedded between two higher-K zones forms a layered sedimentary aquifer structure above 387 m. A sharp boundary at 390.5 m separates this low-K zone from the most permeable structure above. In contrast, the high permeability layer at 388 m shows smooth boundaries. It is not horizontal, but it shows a slight dip toward P11. A zone with very low-K values is visible at the bottom right side of the profile below 387 m. Beneath this low-K zone, a slight increase of K is found. This barely visible permeable structure provides the connection between the deepest injection and upper observation points, where breakthrough was detected (see Figure 6b). The bottom left side of the tomogram exhibits high-K values. The thermal Péclet number even at the lowest inverted K values is still above 1, meaning that advection is the dominant transport process in every part of the aquifer.

Unreliable parts of the tomogram are masked out based on the null-space energy map. The null-space energy map in Figure 7b is calculated from the inverted transport pathways. Therefore, it reveals which parts of the profile were accessed by the thermal tracer. The low-K zone at 386 m for example exhibits a higher null-space compared to adjacent layers above and below, indicating that fewer transport pathways exist in this zone. Compared to other studies [Jiménez et al., 2013; Somogyvári et al., 2016], a null-space energy value of 50% was selected as a threshold for reliable pixels. This value is much lower than previous studies (where e.g., 90% was suggested) because the inversion used fewer BTCs and coarser grid resolution. The reliability of the pixels changes gradually toward the edges of the tomogram. This makes it difficult to find a suitable null-space limit value compared to synthetic studies where this transition was sharper.

To validate the tomogram, first the reconstructed *K* values from well P11 are compared with multilevel slug test results from multiple wells nearby (Figure 8a). The slug tests were performed with 0.3 m spatial resolution over a screen length of 0.3 m (without overlapping intervals) [*Jimenez et al.*, 2016]. The derived profiles show similar vertical trends, but with different local features. While the slug test profiles show sudden changes between the tested intervals, the vertical changes in the tomogram are smooth. All profiles reach the minimum values close to 390 m, but in the slug test profiles this low-*K* zone is narrower. An additional low-*K* peak is visible at 387 m in the tomogram profile, which cannot be correlated with local minimums of

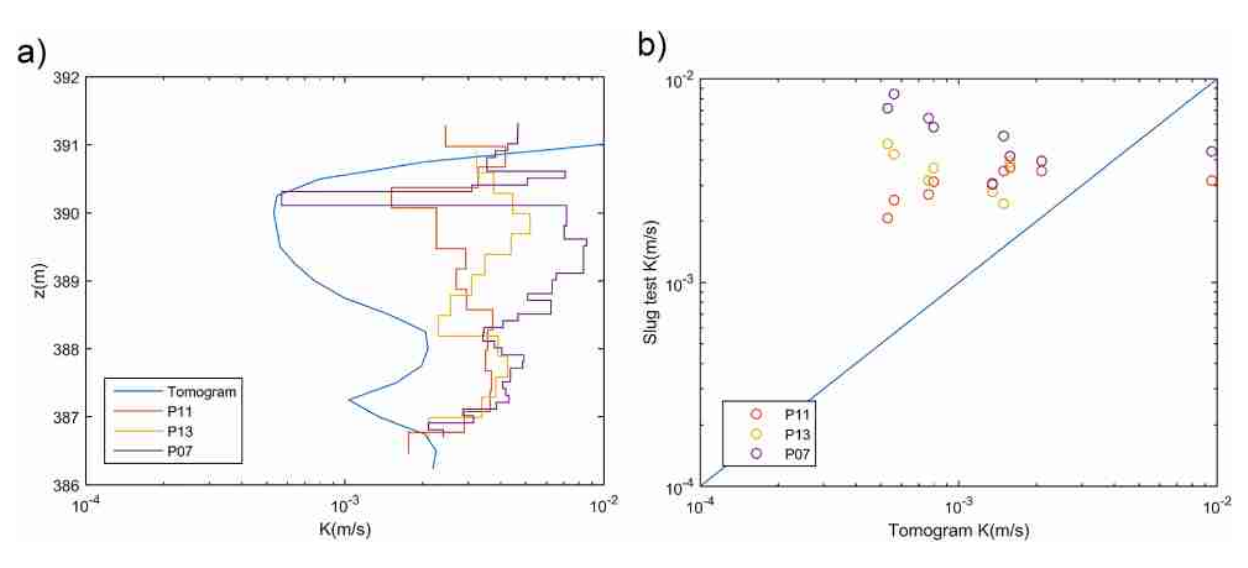


Figure 8. Validation of the reconstructed hydraulic conductivities, K. (a) Comparison of different hydraulic conductivity profiles. One profile is extracted from the K-tomogram at the location of well P11 and compared with slug tests from wells P11, P13, and P07 [Jiménez et al., 2016]. (b) Scatterplot for the comparison of the K values of the tomogram and slug tests.

the slug test profiles. The main difference between the slug tests and the tomogram is visible between 388 and 390 m, due to the large thickness of the low-K layer in the tomographic reconstruction. The inverted K values in the tomogram are lower than the values from the slug tests. This corresponds with the findings by *Somogyvári et al.* [2016], where thermal tracer-based tomograms underestimated the K of the tested synthetic aquifers. This could be explained by the limitations of the assumption of purely advective heat transport. The K-profile extracted from the tomogram changes over 1 order of magnitude. The range covered by the slug tests is significantly smaller. While thermal tracer tomography uses point sources and receivers and is only sensitive toward the flow direction, slug tests integrate K over the entire used screen length in 360°. This integrative behavior suppresses any large changes in the slug test profile, which apparently is better revealed by the thermal tracer tomography. Tomographic methods capture larger-scale heterogeneities than localized slug tests [*Vesselinov et al.*, 2001a, 2001b]. The difference in the reconstructed K values is even more visible in the scatterplot shown in Figure 8b.

Compared to the findings of previous geophysical measurements [Doetsch et al., 2010; Coscia et al., 2011], the biggest difference is that the tomogram shows the highest K values above 390.5 m, while the ERT measurements suggested high-K values between 387.5 and 390 m. The slug test result from P11 supports the result of the tomography (see Figure 8) since it shows the highest K values above 390 m as well. Note that this zone is very close to the water table level (391.8 m on the first day of the thermal tracer tomography campaign, similar for ERT measurements), which could cause artifacts in electric measurements for the ERT. The boundaries of both the thermal tracer tomography and the ERT reconstructions are close to this level, which could lead to less reliable results.

The tomogram of Figure 7 reveals a high-K layer in the center of the aquifer between 387.5 and 389 m which is in agreement with the geophysical results. Its inverted K value of 2×10^{-3} m/s is close to the 1.6 $\times 10^{-3}$ m/s value found by Jiménez et al. [2016] using joint inversion of solute tracer tomography and multilevel slug tests. So far, no hydraulic tomography experiment was performed at the same location. The same study suggested the presence of an extensive thin low-K sand layer at 390 m depth. This layer is also visible in the tomogram at the same depth but is thicker. The cause of this difference may be that thermal tracer tomography tends to reduce high-K and increase low-K zones [Somogyvári et al., 2016]. The inversion by Jiménez et al. [2016] was also performed jointly with slug tests, and the slug test profile indicated a very thin sand layer at 390 m (see Figure 8).

The inverted K values for the sand layer (around 4×10^{-4} m/s) in Figure 7 are close to the values found by Jiménez et al. [2016] for the same feature (3 \times 10⁻⁴ m/s). The final K values of the tomogram are scaled by the used hydraulic gradient, porosity, and heat capacity values, and any changes in these parameters would

result in changes of the final result. However, these changes are always small, because these parameters do not span orders of magnitudes and they are linear multipliers in the *K* calculation (see equation (1)).

Although it was not known prior to the experiment, further indications of the deep low-K zone at 386 m have been found by the recent tracer tomography study performed within the project of Kittilä et al. [2016]. In their experiment, a low-K zone was reconstructed in an adjacent profile (between MC1 and MC3) at a similar depth. The low-K zone can be explained by the presence of a sand lens, similar to the one known from well P3. This sand lens is very close to the aquifer bottom, but the tomogram shows that a thin conductive channel separates them. The bottom boundary identified in the tomogram matches with the aquifer bottom geometry known from core logs. Here the null-space energy values show an abrupt increase, as no transport pathway penetrates the low-K aquifer bed. Therefore, this basal formation was not reconstructed.

5. Conclusions

Motivated by the promising results with synthetic cases, the presented work examined the suitability of travel time-based thermal tracer tomography in a field case. However, field experiments with multiple injections of heat can be technically demanding and time consuming. Hence, a core issue was the development of a fast, simple, and cost-effective test design, which would facilitate the first inversion of a thermal tracer tomogram in the field. As a test site, a heterogeneous alluvial aquifer was chosen, which was already investigated previously in field campaigns. By focusing on a small, 7 m deep cross section between two boreholes around 1.20 m apart, short-term and multilevel warm water injections in the one borehole were sufficient to detect different thermal breakthroughs in the downstream observation borehole. This saved time, equipment, and heating devices, which would be required for more extensive continuous injections. Nevertheless, this also required modifications to the available travel time-based inversion procedure, which was originally developed for long-term injection. The new formulation is suitable for pulse injections and it also offers a way to approximate thermal breakthrough time from temperature-time derivatives. The approximation underestimates the real breakthrough time due to thermal diffusion. Thus, it is only suggested here for estimating late breakthroughs, which are utilized to complement measured breakthroughs, ultimately obtaining a more complete data set for tomographic inversion.

The chosen thermal pulse signals were employed sequentially over 3 days between the multilevel sources and receivers and the recorded signals in the downgradient observation borehole indicated major connections. In the experiment, forced gradient conditions were applied to establish a controlled flow regime with advection-dominated transport. This allowed a travel time-based tomographic inversion of the tracer breakthroughs to reconstruct hydraulic aquifer heterogeneity. A premise for applying this procedure is that further physical parameters that influence heat transport in porous media can be predetermined or neglected. In that case, only the spatial *K* distribution governs the propagation of the thermal pulse in the aquifer.

The inverted tomogram was compared to findings from previous investigations at the field site and showed that similar features were captured by thermal tracer tomography. In particular, a known central low-*K* layer and the steep aquifer bed were successfully reconstructed on the tomogram. In addition, the magnitudes of inverted *K* values are consistent with those from earlier hydraulic field investigations. A low conductivity zone in the tomogram at the bottom part of the aquifer is interpreted as a sand lens or local sandy zone, which is a common feature of the gravel hosting the aquifer. This is also validated by a recent field investigation with colloid tracers.

The presented thermal tracer tomography design provides a cost-effective alternative to using other tracers, like solute tracers for instance. Although the experimental times are longer because of the slower propagation of thermal signals, the recorded temperature breakthrough curves can be obtained real time with highly sensitive sensors or DTS. The observed temperature breakthrough curves exhibit low noise and are thus ideal for travel time detection. For investigation of greater aquifer volumes, the thermal signals need to be adjusted, either by longer injection times or by higher temperature. Here the challenge would be finding the balance between the amount of heat per injection and the temperature recovery time of the aquifer.

Thermal tracer tomography can be performed in par with hydraulic tomography experiments. The joint inversion of these two test types could potentially increase the quality of reconstruction without significantly increasing the experimental costs.

Acknowledgments

This study was supported by the Swiss National Science Foundation under grant 200021_149128. The field experiments at the Widen site has been conducted as part of the RECORD Catchment project. We thank Berrak Firat and Mischa Schweingruber for the help in conducting the field campaigns, and Rachael Colldeweih for language corrections. All data is available by e-mailing the corresponding author (mark. somogyvari@erdw.ethz.ch).

References

- Anderson, M. P. (2005), Heat as a ground water tracer, Ground Water, 43(6), 951-968, doi:10.1111/j.1745-6584.2005.00052.x.
- Aster, R. C., B. Borchers, and C. H. Thurber (2013), Parameter Estimation and Inverse Problems, Academic, Oxford, U. K.
- Bakker, M., R. Caljé, F. Schaars, K.-J. van der Made, and S. de Haas (2015), An active heat tracer experiment to determine groundwater velocities using fiber optic cables installed with direct push equipment, *Water Resour. Res.*, 51, 2760–2772, doi:10.1002/2014WR016632.
- Bense, V. F., T. Read, O. Bour, T. Le Borgne, T. Coleman, S. Krause, A. Chalari, M. Mondanos, F. Ciocca, and J. S. Selker (2016), Distributed temperature sensing as a downhole tool in hydrogeology, *Water Resour. Res.*, 52, 9259–9273, doi:10.1002/2016WR018869.
- Benz, S. A., P. Bayer, K. Menberg, S. Jung, and P. Blum (2015), Spatial resolution of anthropogenic heat fluxes into urban aquifers, Sci. Total Environ., 524 525–, 427–439, doi:10.1016/j.scitotenv.2015.04.003.
- Berg, S. J., and W. A. Illman (2011), Capturing aquifer heterogeneity: Comparison of approaches through controlled sandbox experiments, Water Resour. Res., 47, W09514, doi:10.1029/2011WR010429.
- Brauchler, R., R. Liedl, and P. Dietrich (2003), A travel time based hydraulic tomographic approach, *Water Resour. Res.*, 39(12), 1370, doi: 10.1029/2003WR002262.
- Brauchler, R., G. Böhm, C. Leven, P. Dietrich, and M. Sauter (2013a), A laboratory study of tracer tomography, *Hydrogeol. J., 21*(6), 1265–1274, doi:10.1007/s10040-013-1006-z.
- Brauchler, R., R. Hu, L. Hu, S. Jiménez, P. Bayer, P. Dietrich, and T. Ptak (2013b), Rapid field application of hydraulic tomography for resolving
- aquifer heterogeneity in unconsolidated sediments, *Water Resour. Res.*, 49, 2013–2024, doi:10.1002/wrcr.20181.

 Butler, J. J., C. D. McElwee, and G. C. Bohling (1999), Pumping tests in networks of multilevel sampling wells: Motivation and methodology, *Water Resour. Res.*, 35(11), 3553–3560, doi:10.1029/1999WR900231.
- Cardiff, M., W. Barrash, P. K. Kitanidis, B. Malama, A. Revil, S. Straface, and E. Rizzo (2009), A potential-based inversion of unconfined steady-state hydraulic tomography, *Ground Water*, 47(2), 259–270, doi:10.1111/j.1745-6584.2008.00541.x.
- Cherubin, C., N. Pastore, C. I. Giasi, and N. M. Aldegretti (2017), Laboratory experimental investigation of heat transport in fractured media,
- Nonlinear Process. Geophys., 24(1), 23–42, doi:10.5194/npg-24-23-2017.
 Coleman, T. I., B. L. Parker, C. H. Maldaner, and M. J. Mondanos (2015), Groundwater flow characterization in a fractured bedrock aquifer
- using active DTS tests in sealed boreholes, *J. Hydrol.*, *528*, 449–462, doi:10.1016/j.jhydrol.2015.06.061.
 Colombani, N., B. M. S. Giambastiani, and M. Mastrocicco (2015), Combined use of heat and saline tracer to estimate aquifer properties in a
- forced gradient test, *J. Hydrol.*, *525*, 650–657, doi:10.1016/j.jhydrol.2015.04.026.
 Coscia, I., S. A. Greenhalgh, N. Linde, J. Doetsch, L. Marescot, T. Günther, T. Vogt, and A. G. Green (2011), 3D crosshole ERT for aquifer char-
- acterization and monitoring of infiltrating river water, *Geophysics*, *76*(2), G49.

 Datta-Gupta, A., S. Yoon, D. W. Vasco, and G. A. Pope (2002), Inverse modeling of partitioning interwell tracer tests: A streamline approach, *Water Resour. Res.*, *38*(6). doi:10.1029/2001WR000597.
- Djibrilla Saley, A., A. Jardani, A. Soueid Ahmed, A. Raphael, and J. P. Dupont (2016), Hamiltonian Monte Carlo algorithm for the characterization of hydraulic conductivity from the heat tracing data, *Adv. Water Resour.*, 97, 120–129, doi:10.1016/j.advwatres.2016.09.004.
- Doetsch, J., N. Linde, I. Coscia, S. A. Greenhalgh, and A. G. Green (2010), Zonation for 3D aquifer characterization based on joint inversions of multimethod crosshole geophysical data, *Geophysics*, 75(6), G53–G64, doi:10.1190/1.3496476.
- Dorn, C., N. Linde, T. Le Borgne, O. Bour, and J. R. de Dreuzy (2013), Conditioning of stochastic 3-D fracture networks to hydrological and geophysical data, *Adv. Water Resour.*, 62(PA), 79–89, doi:10.1016/j.advwatres.2013.10.005.
- Doro, K. O., O. A. Cirpka, and C. Leven (2015), Tracer tomography: Design concepts and field experiments using heat as a tracer, *Ground Water*, *53*(51), 139–148, doi:10.1111/gwat.12299.
- Einarson, M. D., and J. A. Cherry (2002), A new multilevel ground water monitoring system using multichannel tubing, *Ground Water Monit. Remediat.*, 22(4), 52–65, doi:10.1111/j.1745-6592.2002.tb00771.x.
- Evans, G. V. (1983), Tracer techniques in hydrology, *Int. J. Appl. Radiat. Isot.*, *34*(1), 451–475, doi:10.1016/0020-708X(83)90144-8.
- Feehley, C. E., C. Zheng, and F. J. Molz (2000), A dual-domain mass transfer approach for modeling solute transport in heterogeneous aquifers: Application to the Macrodispersion Experiment (MADE) site, Water Resour. Res., 36(9), 2501–2515, doi:10.1029/2000WR900148.
- Hu, L., P. Bayer, P. Alt-Epping, A. Tatomir, M. Sauter, and R. Brauchler (2015), Time-lapse pressure tomography for characterizing CO₂ plume evolution in a deep saline aquifer, *Int. J. Greenhouse Gas Control*, 39, 91–106, doi:10.1016/j.ijggc.2015.04.013.
- Illman, W. A., X. Liu, S. Takeuchi, T.-C. J. Yeh, K. Ando, and H. Saegusa (2009), Hydraulic tomography in fractured granite: Mizunami Underground Research site, Japan, *Water Resour. Res.*, 45, W01406, doi:10.1029/2007WR006715.
- Illman, W. A., S. J. Berg, X. Liu, and A. Massi (2010), Hydraulic/partitioning tracer tomography for DNAPL source zone characterization: Small-scale sandbox experiments, *Environ. Sci. Technol.*, 44(22), 8609–8614, doi:10.1021/es101654j.
- Irvine, D. J., C. T. Simmons, A. D. Werner, and T. Graf (2013), Heat and solute tracers: How do they compare in heterogeneous aquifers?, *Ground Water*, 53, 10–20, doi:10.1111/gwat.12146.
- Jackson, M. J., and D. R. Tweeton (1996), 3DTOM, Three-Dimensional Geophysical Tomography, U.S. Dep. of the Inter., Bur. of Mines, Twin Cities. Minn.
- Jiménez, S., R. Brauchler, and P. Bayer (2013), A new sequential procedure for hydraulic tomographic inversion, *Adv. Water Resour.*, 62(PA), 59–70, doi:10.1016/j.advwatres.2013.10.002.
- Jiménez, S., R. Brauchler, R. Hu, L. Hu, S. Schmidt, T. Ptak, and P. Bayer (2015), Prediction of solute transport in a heterogeneous aquifer utilizing hydraulic conductivity and specific storage tomograms, *Water Resour. Res.*, 51, 5504–5520, doi:10.1002/2014WR016402.
- Jiménez, S., G. Mariethoz, R. Brauchler, and P. Bayer (2016), Smart pilot points using reversible-jump Markov-chain Monte Carlo, Water Resour. Res., 52, 3966–3983, doi:10.1002/2015WR017922.
- Keys, W. S., and R. F. Brown (1978), The use of temperature logs to trace the movement of injected water, *Ground Water*, 16, 32–48, doi: 10.1111/j.1745-6584.1978.tb03201.x.
- Kittilä, A., K. Evans, M. Puddu, G. Mikutis, R. N. Grass, C. Deuber, and M. O. Saar (2016), The use of novel DNA nanotracers to determine groundwater flow paths-a test study at the Grimsel Deep Underground Geothermal (DUG) Laboratory in Switzerland, in EGU General Assembly Conference Abstracts, vol. 18, p. 16204, Vienna, Austria.

- Klepikova, M. V., T. Le Borgne, O. Bour, K. Gallagher, R. Hochreutener, and N. Lavenant (2014), Passive temperature tomography experiments to characterize transmissivity and connectivity of preferential flow paths in fractured media, J. Hydrol., 512, 549–562, doi: 10.1016/j.jhydrol.2014.03.018.
- Linde, N., J. Chen, M. B. Kowalsky, and S. Hubbard (2006), Hydrogeophysical parameter estimation approaches for field scale characterization, in *Applied Hydrogeophysics*, vol. i, pp. 9–44, Springer, Dordrecht, Netherlands.
- Molz, F. J., A. D. Parr, and P. F. Andersen (1981), Thermal energy storage in a confined aquifer: Second cycle, *Water Resour. Res.*, 17(3), 641, doi:10.1029/WR017i003p00641.
- Oppenheim, A. V., and J. S. Lim (1981), The importance of phase in signals, Proc. IEEE, 69(5), 529-541, doi:10.1109/PROC.1981.12022.
- Palmer, C. D., D. W. Blowes, E. O. Frind, and J. W. Molson (1992), Thermal energy storage in an unconfined aquifer: 1. Field injection experiment, Water Resour. Res., 28(10), 2845–2856, doi:10.1029/92WR01471.
- Rau, G. C., M. S. Andersen, A. M. McCallum, H. Roshan, and R. I. Acworth (2014), Heat as a tracer to quantify water flow in near-surface sediments. *Earth Sci. Rev.*. 129, 40–58. doi:10.1016/j.earscirev.2013.10.015.
- Saar, M. O. (2011), Review: Geothermal heat as a tracer of large-scale groundwater flow and as a means to determine permeability fields, Hydrogeol. J., 19(1), 31–52, doi:10.1007/s10040-010-0657-2.
- Sanchez-León, E., C. Leven, C. P. Haslauer, and O. A. Cirpka (2016), Combining 3D hydraulic tomography with tracer tests for improved transport characterization, *Ground Water*, 54(4), 498–507, doi:10.1111/gwat.12381.
- Schincariol, R. A., and F. W. Schwartz (1990), An experimental investigation of variable density flow and mixing in homogeneous and heterogeneous media, Water Resour. Res., 26(10), 2317–2329, doi:10.1029/90WR01161.
- Schwede, R. L., W. Li, C. Leven, and O. A. Cirpka (2014), Three-dimensional geostatistical inversion of synthetic tomographic pumping and heat-tracer tests in a nested-cell setup, *Adv. Water Resour.*, 63, 77–90, doi:10.1016/j.advwatres.2013.11.004.
- Schweingruber, M., M. Somogyvári, and P. Bayer (2015), Active thermal tracer testing in a shallow aquifer of the Thur valley, Switzerland, EGU General Assembly Conference Abstracts, vol. 17, p. 9590, Vienna.
- Seibertz, K. S. O., M. A. Chirila, J. Bumberger, P. Dietrich, and T. Vienken (2016), Development of in-aquifer heat testing for high resolution subsurface thermal-storage capability characterisation, *J. Hydrol.*, 534, 113–123, doi:10.1016/j.jhydrol.2015.12.013.
- Sharmeen, R., W. A. Illman, S. J. Berg, T.-C. J. Yeh, Y.-J. Park, E. A. Sudicky, and K. Ando (2012), Transient hydraulic tomography in a fractured dolostone: Laboratory rock block experiments, *Water Resour. Res.*, 48, W10532, doi:10.1029/2012WR012216.
- Shook, G. M. (2001), Predicting thermal breakthrough in heterogeneous media from tracer tests, Geothermics, 30(6), 573–589.
- Somogyvári, M., P. Bayer, and R. Brauchler (2016), Travel-time-based thermal tracer tomography, *Hydrol. Earth Syst. Sci.*, 20(5), 1885–1901, doi:10.5194/hess-20-1885-2016.
- Stauffer, F., P. Bayer, P. Blum, N. M. Giraldo, and W. Kinzelbach (2013), *Thermal Use of Shallow Groundwater*, CRC Press, Boca Raton, Fla. Vandenbohede, A., T. Hermans, F. Nguyen, and L. Lebbe (2011), Shallow heat injection and storage experiment: Heat transport simulation and sensitivity analysis, *J. Hydrol.*, 409(1–2), 262–272, doi:10.1016/j.jhydrol.2011.08.024.
- Vasco, D. W., and A. Datta-Gupta (1999), Asymptotic solutions for solute transport: A formalism for tracer tomography, *Water Resour. Res.*, 35(1), 1–16. doi:10.1029/98WR02742.
- Vasco, D. W., and S. Finsterle (2004), Numerical trajectory calculations for the efficient inversion of transient flow and tracer observations, Water Resour. Res., 40, W01507, doi:10.1029/2003WR002362.
- Vasco, D. W., H. Keers, and K. Karasaki (2000), Estimation of reservoir properties using transient pressure data: An asymptotic approach, Water Resour. Res., 36(12), 3447–3465, doi:10.1029/2000WR900179.
- Vesnaver, A., and G. Böhm (2000), Staggered or adapted grids for seismic tomography?, Lead. Edge, 19(9), 944, doi:10.1190/1.1438762.
- Vesselinov, V. V, S. P. Neuman, and W. A. Illman (2001a), Three-dimensional numerical inversion of pneumatic cross-hole tests in unsaturated fractured tuff: 1. Methodology and borehole effects, Water Resour. Res., 37(12), 3001–3017, doi:10.1029/2000WR000133.
- Vesselinov, V. V., S. P. Neuman, and W. A. Illman (2001b), Three-dimensional numerical inversion of pneumatic cross-hole tests in unsaturated fractured tuff: 2. Equivalent parameters, high-resolution stochastic imaging and scale effects, Water Resour. Res., 37(12), 3019–3041, doi:10.1029/2000WR000135.
- Wagner, V., T. Li, P. Bayer, C. Leven, P. Dietrich, and P. Blum (2014), Thermal tracer testing in a sedimentary aquifer: Field experiment (Lauswiesen, Germany) and numerical simulation. *Hydrogeol. J.*, 22(1), 175–187. doi:10.1007/s10040-013-1059-z.
- Wildemeersch, S., P. Jamin, P. Orban, T. Hermans, M. Klepikova, F. Nguyen, S. Brouyère, and A. Dassargues (2014), Coupling heat and chemical tracer experiments for estimating heat transfer parameters in shallow alluvial aquifers, *J. Contam. Hydrol.*, 169, 90–99, doi:10.1016/i.iconhvd.2014.08.001.
- Xie, Y., P. G. Cook, C. T. Simmons, and C. Zheng (2015), On the limits of heat as a tracer to estimate reach-scale river-aquifer exchange flux, Water Resour. Res., 51, 7401–7416, doi:10.1002/2014WR016741.
- Xue, Y., C. Xie, and Q. Li (1990), Aquifer thermal energy storage: A numerical simulation of field experiments in China, *Water Resour. Res.*, 26(10), 2365–2375, doi:10.1029/WR026i010p02365.
- Yeh, T.-C. J., and J. Zhu (2007), Hydraulic/partitioning tracer tomography for characterization of dense nonaqueous phase liquid source zones, *Water Resour. Res.*, 43, W06435, doi:10.1029/2006WR004877.
- Zhu, J., X. Cai, and T.-C. Jim Yeh (2009), Analysis of tracer tomography using temporal moments of tracer breakthrough curves, *Adv. Water Resour.*, 32(3), 391–400, doi:10.1016/j.advwatres.2008.12.001.

19447973, 2017, 6, Downloaded from https://agupubs.onlinelibrary.wiley.com/doi/10.1002/2017WR020543 by Cochrane Germany, Wiley Online Library on [22/08/2023]. See the Terms and Conditions (https://onlinelibrary.wiley.com/terms-and-conditions) on Wiley Online Library for rules of

use; OA articles